Dynamics and spin relaxation of excitons in GaAs/$Al_xGa_{1-x}As$ quantum wells

A. Frommer,* Arza Ron, and E. Cohen
Solid State Institute, Technion-Israel Institute of Technology, Haifa 32000, Israel

J. A. Kash
IBM Research Division, Thomas J. Watson Research Center, Yorktown Heights, New York 10598

L. N. Pfeiffer
AT&T Bell Laboratories, Murray Hill, New Jersey 07974

(Received 19 August 1993; revised manuscript received 18 July 1994)

We present a study of the optical spin orientation and optical alignment relaxation of ($e1$:hh1)1S excitons in GaAs/$Al_{0.33}Ga_{0.67}As$ narrow quantum wells at low temperatures. The photoluminescence was excited by ps pulses within the ($e1$:hh1) exciton band and its decay, as well as that of the degrees of the circular and linear polarizations [$P_{cir}(t)$ and $P_{lin}(t)$] were measured. The observed decay curves are analyzed by a model based on the in-plane wave-vector ($\mathbf{K}_\parallel$) dependence of the energy (τ_a), spin (τ_{cir}), and alignment (τ_{lin}) relaxation times of delocalized excitons. These were found to vary in the range of $120<\tau_a<230$ ps, $50>\tau_{cir}>30$ ps, and $15>\tau_{lin}>5$ ps for 0.019 $Å^{-1}<K_\parallel<0.032$ $Å^{-1}$. The model fitting is not sensitive to the relaxation times of the $K_\parallel=0$ state, which are very long: $1000>\tau^0_{lin},\tau^0_{cir}>300$ ps. We further assume that the hole spin-relaxation rate is much faster than that of the electron. This allows us to estimate the relative contribution of each of these particles' spin-relaxation rate to τ_{cir} and τ_{lin}.

I. INTRODUCTION

The dynamics of excitons in quantum wells (QW's) and their effect on the photoluminescence (PL) spectrum has been extensively studied in recent years.[1–8] Various nonlinear techniques such as hole burning and transient grating spectroscopy have been used in order to study exciton dephasing in GaAs/$Al_xGa_{1-x}As$ heterostructures.[9–11] The degree of polarization P, which is observed in the PL spectrum of e-h pair recombination under optical pumping conditions, has been shown to be a powerful tool in determining the dynamic processes which the e-h pair undergoes during the stages of photoexcitation, energy relaxation, and radiative recombination, both in bulk semiconductors[12,13] and in QW's.[14,15] Several recent reports [16–19] examined the temporal dependence of the degree of circular polarization P_{cir} in the spectral range of the ($e1$:hh1)1S PL band. Due to the great complications arising from the fact that the electron and hole are coupled within the exciton (in both their orbital motion and their spins), the results were analyzed in terms of separate particle spin-relaxation rates. Then, assuming a much faster spin relaxation for the hole part of the excitonic wave function than that of the electron part, P_{cir} in undoped samples is determined by the more slowly relaxing electron. In doped semiconductors the spin orientation of the photoexcited majority carriers is assumed to be lost in the degenerate Fermi sea, and the observed relaxation of P_{cir} is determined by the spin relaxation of the photoexcited minority carriers. Some observations indicate that an additional polarization is observed due to electron-electron collisions that mix the electrons and can give a net polarization to the Fermi-sea electrons.[16] The hole spin-relaxation time, which was experimentally determined by measuring P_{cir} in n-doped QW's,[16] was analyzed theoretically[12,20,21] and was shown to be determined by valence subband mixing. The degree of linear polarization P_{lin} differs from P_{cir} in that any scattering process which changes either the electron or the hole state, or relaxes the spin coherence between them, results in a complete loss of the exciton linear polarization.[12,22] A study of $P_{lin}(t)$ for an undoped QW excited selectively in the ($e1$:hh1) PL band indicated that exciton relaxation processes preserve some degree of linear polarization.[23] All these studies showed that $P_{cir}(t)$ and $P_{lin}(t)$ are sensitive probes of the exciton states and the dynamic processes in which the exciton is involved.

The underlying principles of the polarization properties of free excitons are derived from the following symmetry considerations. The heavy-hole valence (conduction) band $\mathbf{k}=0$ states are p-like (s-like), with a total angular momentum $J=\frac{3}{2}, J_z=\pm\frac{3}{2}$ ($J=\frac{1}{2}$, $J_z=\pm\frac{1}{2}$). Among the four possible exciton states with the 1S envelope, two are optically allowed (Γ_5 symmetry), and two are optically forbidden (Γ_6 symmetry). They are denoted by $|+1\rangle=|-\frac{1}{2},+\frac{3}{2}\rangle$, $|-1\rangle=|+\frac{1}{2},-\frac{3}{2}\rangle$, and by $|+2\rangle=|+\frac{1}{2},+\frac{3}{3}\rangle$, $|-2\rangle=|-\frac{1}{2},-\frac{3}{2}\rangle$, respectively. $|m_j^e,m_j^h\rangle$ denotes the states with angular momentum projection m_j^e and m_j^h of the electron and the hole along the growth (z) direction, respectively. The $|\pm1\rangle$ notation for the optically allowed excitons indicates that the light may transfer a total momentum of $\Delta J_z=\pm1$ to the crystal. Therefore light propagating along the z direction and is circularly polarized $\sigma^+(\sigma^-)$ creates $|+1\rangle(|-1\rangle)$ excitons. Similarly, linearly polarized light along the x direction creates $|x\rangle=(1/\sqrt{2})(|+1\rangle+|-1\rangle)$ excitonic states and light polarized along the y direction creates

$|y\rangle=(1/\sqrt{2})(|+1\rangle-|-1\rangle)$ excitonic states.[22] Thus, in this case, neither the electron nor the hole are oriented by themselves, and the linear polarization is a property of the e-h pair. Depolarization of one of the particles or loss of the spin coherence between them will destroy the whole pair polarization. For $\mathbf{K}\neq 0$ excitonic states additional complications arise due to the increased admixture of the bands, and a more rapid spin relaxation is expected.[12,17,20,21] This effect is much stronger for the valence band states since subband mixing and the spin-orbit interaction are strong.

In this work we studied the temporal dependence of $P_{\rm cir}$ and $P_{\rm lin}$ by monitoring the PL at the peak of the $(e1{:}{\rm hh}1)1S$ exciton band and selectively exciting at various energies within the excitonic band in GaAs/Al_xGa_{1-x}As multiple QW's. We studied both $P_{\rm lin}(t)$ and $P_{\rm cir}(t)$ and the comparison between them in order to identify the dynamic processes which preserve the exciton polarization. We consider the exciton center-of-mass motion (in the QW plane) in the fluctuating potential that is due to interface roughness and barrier alloy fluctuations. We analyze the decay curves by assuming that the excitons involved are "delocalized", [24] namely, that their in-plane motion can be approximated by a defined in-plane wave vector $\mathbf{K}_{\|}$. Furthermore, we assume that at moderate excitation intensities most of the light emitted at the peak of the PL line is due to these delocalized excitons. We distinguish between $1S$ and $2S$ inhomogeneously broadened $K_{\|}\approx 0$ excitonic bands observed in the PL spectra, and find that $K_{\|}$-dependent energy- and spin-relaxation times determine the PL and the polarization decay curves. The analysis demonstrates the importance of both the translational and the internal excitonic states in determining the degree of polarization. Assuming that the hole spin-relaxation rate is much faster than that of the electron, we estimate the relative contribution of each of these particles' spin-relaxation rate to the circular and linear polarization relaxation rate.

The paper is laid out as follows. In Sec. II we give a brief description of the experimental procedure and results. Section III presents a model of photoexcited exciton dynamics and polarization relaxation and a fit to the experimentally determined decay curves. Our main results and conclusions are summarized in Sec. IV.

II. EXPERIMENT

We studied a nominally undoped GaAs/$As_{0.33}Ga_{0.67}$As MQW grown by molecular-beam epitaxy on a (001)-oriented semi-insulating GaAs substrate. The sample has 50 Å wells, 200 Å barriers, and 50 periods. It was placed in an immersion-type dewar, at $T=1.6$ K and a backscattering configuration was used. Time-resolved PL measurements have been performed using a synchronously pumped mode-locked dye laser (pyridine 2) that emitted light pulses of ~6 ps time duration with a repetition rate of 76 MHz and had a maximum power of 40 mW. The luminescence was dispersed by a triple monochromator and analyzed by a time-correlated single photon counting apparatus with a time response of about 60 ps [full width at half maximum (FWHM)]. The laser polarization incident on the sample was modulated with a liquid-crystal polarization rotator, and the PL polarization was analyzed with appropriate linear polarizers and quarter-wave plates.

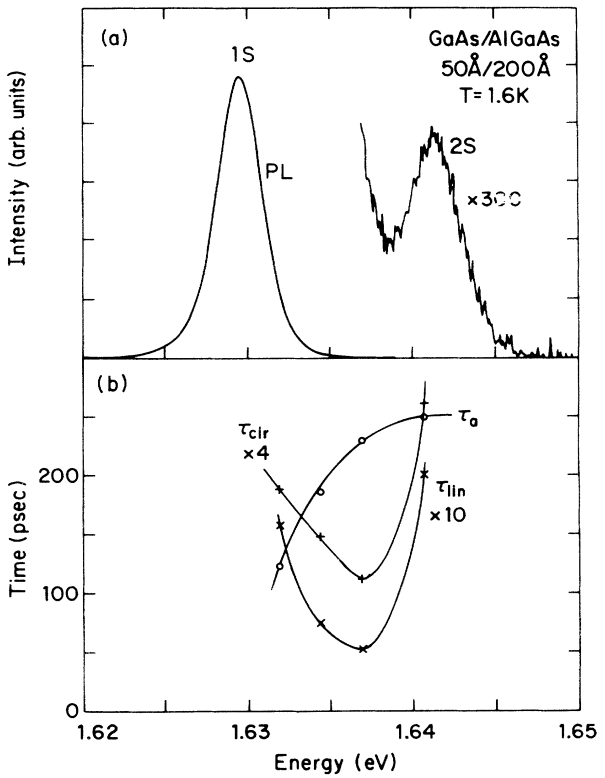

FIG. 1. (a) The photoluminescence spectrum excited deep into the conduction band. (b) The exciton energy-relaxation time τ_a, ○, the spin-relaxation time $\tau_{\rm cir}$, +, and the alignment relaxation time $\tau_{\rm lin}$, ×, for four different excitation energies. $\tau_{\rm cir}$ and $\tau_{\rm lin}$ are multiplied by 4 and 10, respectively. The solid curves joining the time constants are guides to the eye.

Figure 1 shows the time-integrated PL spectrum excited deep into the conduction band. This spectrum consists of the inhomogeneously broadened $1S$ as well as the excited $2S$ band of the $(e1{:}{\rm hh}1)$ exciton. Typical curves of the polarized luminescence decay are shown in Fig. 2. Figure 2(a) shows the right (I_{σ^+}) and left (I_{σ^-}) circularly polarized PL intensity decay for σ^+ excitation. Figure 2(b) shows the decay curves of the PL intensity linearly polarized either parallel ($I_{\|}$) or perpendicular ($I_{\perp}$) to that of the exciting laser. All these spectra were excited at 1.6407 eV and monitored at the peak of the PL spectrum at 1.6292 eV. The time-dependent degree of linear polarization, defined as

$$P_{\rm lin}(t)=[I_{\|}(t)-I_{\perp}(t)]/[I_{\|}(t)+I_{\perp}(t)]\ ,$$

is derived from these curves. $P_{\rm cir}(t)$ is similarly defined and obtained. Figure 3 shows a set of $I_{\rm PL}(t)$, $P_{\rm cir}(t)$, and $P_{\rm lin}(t)$ curves for different energies E_l of the exciting laser. In all these curves the PL was monitored at the

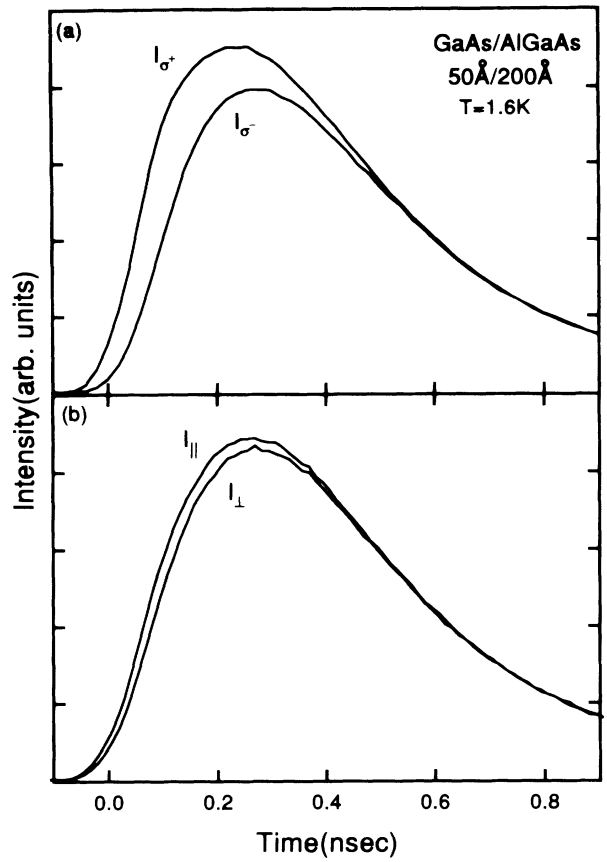

FIG. 2. (a) Time-resolved right ($I_{\sigma+}$) and left ($I_{\sigma-}$) circularly polarized photoluminescence for σ^+ excitation. (b) The same for linearly polarized excitation.

peak of the band, $E_m = 1.6292$ eV. The excitation (laser) intensity in all the experiments was kept at $\sim 2.5 \mathrm{W/cm}^{-2}$.

III. ANALYSIS

We analyze the dependence of $P_{\mathrm{lin}}(t)$ and $P_{\mathrm{cir}}(t)$ on the energy of the exciting laser (E_l) by examining the dynamics of an exciton that is created at E_l and recombines at E_m. Recent studies of the PL band shape[6,7] and of the spectral and temporal dependence of PL (Ref. 8) and of $P_{\mathrm{lin}}(t)$ (Ref. 23) lead to the following description. The spatial potential fluctuations (that are due to interface roughness) can localize the exciton on various length scales. If the localization area is larger than πa_{nS}^2 [where a_{nS} is the Bohr radius of the (e1:hh1)nS state], then the exciton in-plane motion can be approximated by a defined in-plane wave vector, $\mathbf{K}_{\parallel}$. Such areas (often called interface islands) still have short-range roughness[26] that determines the coherence length of all exciton states in a given island. We thus describe the exciton dispersion relations for a given interface island by $E_{1S}(\mathbf{K}_{\parallel}), E_{2S}(\mathbf{K}_{\parallel}), \ldots$ surfaces as shown schematically in Fig. 4(a). Excitons in different interface islands have similar dispersion relations, and they differ only in $E_{1S}(K_{\parallel}=0)$, which is determined by the average potential. We shall refer to these loosely localized excitons as "delocalized."[24] Our study[27] of microwave-modulated PL spectra (of the same sample used here) supports this description of delocalized excitons in the upper part of the PL band. We also note that in a recent communication Schnabel *et al.*[7] explain the exciton PL spectra in $\mathrm{In}_x\mathrm{Ga}_{1-x}\mathrm{As/GaAs}$ QW's by invoking the concept of

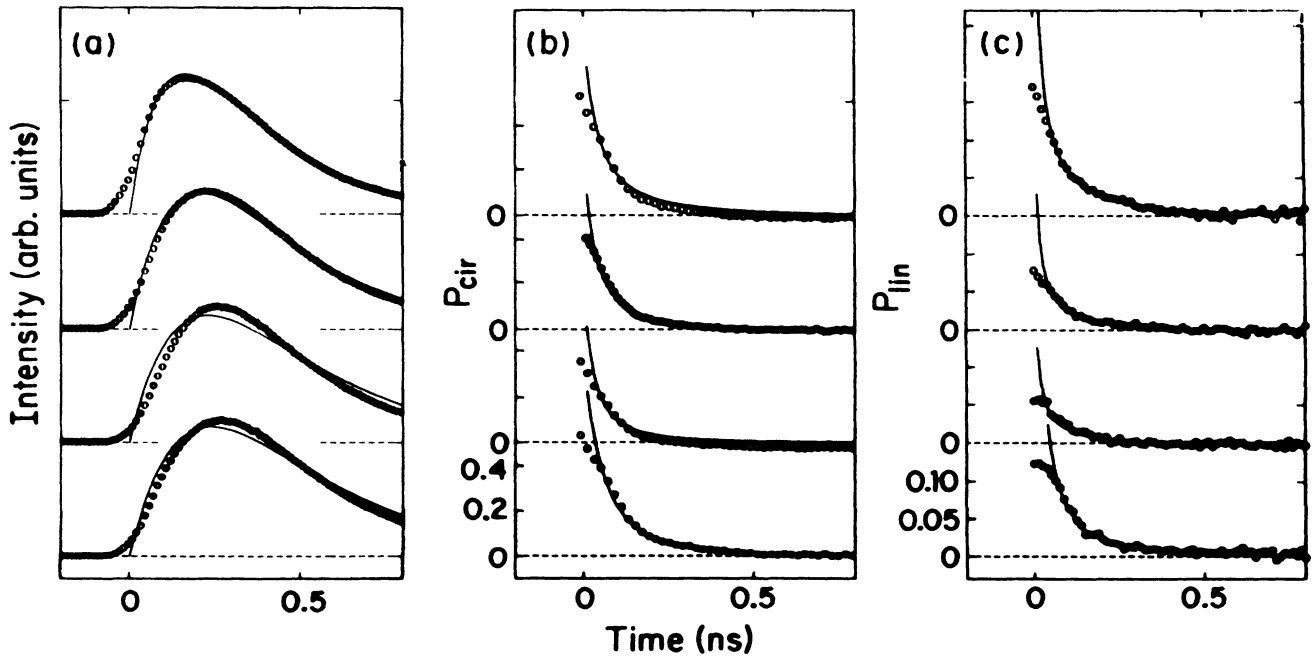

FIG. 3. (a) $I_{\mathrm{PL}}(t)$, (b) $P_{\mathrm{cir}}(t)$, and (c) $P_{\mathrm{lin}}(t)$ (open circles) monitored at the peak of the PL band at $E_m = 1.6292$ eV for four different excitation energies E_l; from top to bottom, 1.6319, 1.6344, and 1.6369 eV within the (e1:hh1)1S band and 1.6407 eV which corresponds to excitation into the (e1:hh1)2S band. The solid curves give the model fit to the experimental results.

"partial localization," which is similar to our description of delocalized excitons. Strictly localized states are those bound to impurities or deep potential fluctuations, and the corresponding exciton energies are in the lowest part of the PL band. Fully extended exciton states are those with energies higher than the PL band.[9] In our samples there is a Stokes shift of the order of [24] ~3 meV between the PL and the absorption bands, indicating that different types of excitonic states contribute to each of them. The PL is emitted only by excitons in the delocalized states and those in strictly localized states. The low-energy part of the absorption which spectrally overlaps the high-energy part of the PL is due to the delocalized excitonic states while the high-energy part of the absorption is due to the extended excitonic states. We will consider here only the polarization of the light emitted at the peak of the PL line (or at higher energies). When using moderate excitation intensities ($I_l \approx 2.5$ W/cm^2) the emitted light in this spectral range corresponds to recombination of delocalized excitons. At lower excitation intensities (4 mW/cm$^2 \leq I_l \leq 0.2$ W/cm^2), different PL and polarization decay times were observed for energies corresponding to the peak of the PL band and below, and a very different polarization spectral behavior was found. The PL at these low excitation intensities is associated with recombination of excitons trapped on impurities. This suggests a density of trapping sites of $\sim 1\times 10^9$ cm^{-2} per quantum well. This is slightly smaller then the $\sim 6\times 10^9$ cm^{-2} suggested by Zucker *et al.*[25] for a 96/98 Å GaAs/$Al_{0.28}Ga_{0.72}As$ MQW deduced from temperature-dependent resonant Raman measurements. The localized excitons behave very differently from the delocalized excitons[24] and their polarization properties will be discussed elsewhere.

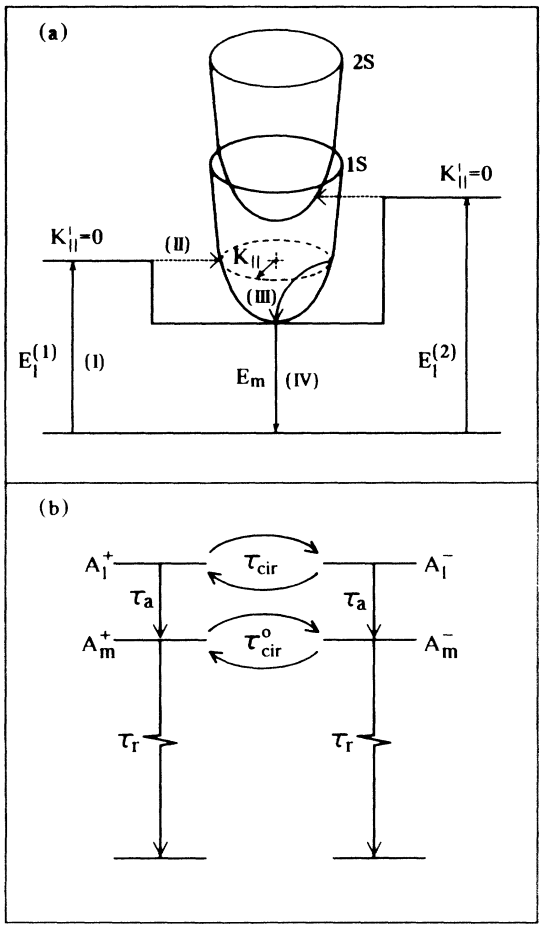

FIG. 4. (a) A schematic description of the model used to interpret the polarization spectra. $E_l^{(1)}$ and $E_l^{(2)}$ are the lowest levels of excitons which are created in the respective interface islands. E_m is the energy at which the exciton radiative recombination is monitored. In this island, the 1*S* and 2*S* dispersion surfaces [$E_{1S}(\mathbf{K}_\|)$ and $E_{2S}(\mathbf{K}_\|)$] are shown. Excitons are transferred from the island where they are created into the one where they recombine so that $E_L^{(1)}=E_{1S}(\mathbf{K}_\|)$ or $E_l^{(2)}=E_{2S}(\mathbf{K}_\|)$. Then they relax into E_m. (I)–(IV) represent the various stages in the exciton life; see text. (b) A schematic energy diagram for the three-level model assumed for the spin-relaxation dynamics.

The dynamic processes which affect $P_{\rm lin}$ and $P_{\rm cir}$ occur in the following stages of the exciton life. (I) Photoexcitation at energy $E_l=E_{1S}(K'_\|=0)$. (II) Elastic scattering from the island with E_l into the one where the exciton recombines. (III) Relaxation into the $K_\|=0$ recombination state within this island. (IV) Recombination at $E_{1S}(K_\|=0)=E_m$. Figure 4(a) schematically shows the various stages in the exciton life in cases where the photoexcited exciton scatters elastically (dotted arrows) into either the 1*S* or the 2*S* band of the interface island with E_m. We assume that the elastic scattering is faster than all other processes involved. The polarization decay curves show a high degree of initial polarization. From this we deduce that in this stage the exciton retains its polarization. Stage (III) of the exciton life is its in-plane motion in a state with a well-defined wave vector $\mathbf{K}_\|$ within the interface island where it relaxes its excess kinetic energy.

Depolarization of excitons having $K_\| = [2M_{\rm ex}(E_l-E_m)/\hbar^2]^{1/2}$, which move in the island where the they recombine, can be induced by elastic scattering processes[12,21] which accompany the excitonic in-plane motion. Depolarization can also occur in the excitonic final state at E_m where *e-h* exchange interaction and spin-orbit coupling determine the spin relaxation of the $K_\| \approx 0$ states.[12] These processes can involve a spin flip of either the hole part or the electron part of the excitonic wave function, or both. In order to extract the circular and linear polarization relaxation times from the observed decay curves, we use a simplified model with a minimal number of parameters which can give a good agreement with the experimental results. In our simplified model we neglect possible intermediate scattering to the $|+2\rangle$ and the $|-2\rangle$ "silent" states. There is no way by which these excitons can be directly observed. We also neglect depolarization during the phonon-assisted energy-relaxation process. Our model is schematically described in Fig. 4(b) [for the case of $P_{\rm cir}(t)$].

We assume a $\delta(t)$-like excitation pulse of σ^+-polarized light and indicate by $A_l^+(t)$, $A_l^-(t)$ and $A_m^+(t)$, $A_m^-(t)$ the populations of $|+1\rangle$ and $|-1\rangle$ excitons with energies E_l

and E_m, respectively. Although we use the same subscripts (l and m) as those used in Fig. 4(a), it should be noted that in Fig 4(b) they refer to the exciton populations within the island where they recombine. Then the exciton dynamics can be described with the following set of rate equations:

$$\frac{dA_l^+}{dt}=G_0\delta(t)-\frac{A_l^+}{\tau_a}-\frac{A_l^+}{\tau_{\rm cir}}+\frac{A_l^-}{\tau_{\rm cir}}\ , \tag{1}$$

$$\frac{dA_l^-}{dt}=-\frac{A_l^-}{\tau_a}-\frac{A_l^-}{\tau_{\rm cir}}+\frac{A_l^+}{\tau_{\rm cir}}\ , \tag{2}$$

$$\frac{dA_m^+}{dt}=-\frac{A_m^+}{\tau_r}+\frac{A_l^+}{\tau_a}-\frac{A_m^+}{\tau_{\rm cir}^0}+\frac{A_m^-}{\tau_{\rm cir}^0}\ , \tag{3}$$

$$\frac{dA_m^-}{dt}=-\frac{A_m^-}{\tau_r}+\frac{A_l^-}{\tau_a}-\frac{A_m^-}{\tau_{\rm cir}^0}+\frac{A_m^+}{\tau_{\rm cir}^0}\ . \tag{4}$$

τ_a is the energy-relaxation time (by acoustic phonon emission) of the exciton at E_l into the state from which it recombines. We showed that τ_a depends on E_l-E_m through the exciton–acoustic-phonon interaction.[24] τ_r is the radiative recombination time of the excitonic state at E_m and is thus independent of E_l. $\tau_{\rm cir}$ and $\tau_{\rm cir}^0$ are the excitonic spin-relaxation times at E_l and E_m ($K_\parallel\sim 0$), respectively. $\tau_{\rm cir}^0$ is due to the spin relaxation of $K_\parallel\sim 0$ excitons (in the spectral range of delocalized excitons) and is thus also independent of E_l.

Integration of Eqs. (1)–(4) yields the following solutions:

$$A_m^+(t)+A_m^-(t)=\frac{G_0}{\tau_a[1/\tau_a-1/\tau_r]}\times[\exp(-t/\tau_r)-\exp(-t/\tau_a)]\ , \tag{5}$$

$$A_m^+(t)-A_m^-(t)=\frac{G_0}{\tau_a[1/\tau_a+2/\tau_{\rm cir}-1/\tau_r-2/\tau_{\rm cir}^0]}\times\left\{\exp\left[-t\left[\frac{1}{\tau_r}+\frac{2}{\tau_{\rm cir}^0}\right]\right]-\exp\left[-t\left[\frac{1}{\tau_a}+\frac{2}{\tau_{\rm cir}}\right]\right]\right\}\ . \tag{6}$$

A similar set of rate equations can be written for the case of $P_{\rm lin}(t)$. $A_l^+(t)$, $A_l^-(t)$, $A_m^+(t)$, and $A_m^-(t)$ are then replaced by $A_l^x(t)$, $A_l^y(t)$, $A_m^x(t)$, and $A_m^y(t)$, respectively, corresponding to $|x\rangle$ and $|y\rangle$ excitonic states with energies E_l and E_m. $\tau_{\rm cir}$ and $\tau_{\rm cir}^0$ are replaced by $\tau_{\rm lin}$ and $\tau_{\rm lin}^0$ associated with the exciton optical alignment relaxation times at E_l and E_m, respectively.

We use our time-resolved PL and polarization measurements in order to extract the relaxation times involved. $I_{\rm PL}(t)\propto A_m^+(t)+A_m^-(t)$, and this determines τ_a and τ_r [by a best fit to the experimental $I_{\rm PL}(t)$]. In Fig. 3(a) we show the fit to the $I_{\rm PL}(t)$ curves, measured with various E_l within the (e1:hh1) spectral range. We obtain $\tau_r=230$ ps, and the energy-relaxation time within the recombining island τ_a, which depends on the (E_l-E_m) separation, increases from 120 to 220 ps when E_l is increased from 1.6319 to 1.6407 eV [Fig. 1(b)]. The increase of τ_a with increasing E_l has been recently[24] shown to be due to the slower exciton–acoustic-phonon relaxation rate for large-$\mathbf{K}_\parallel$ states. The poor fit at very short times after excitation is due to the time resolution of our measuring system and to the fact that the excitation has a finite spread in time. At very short times most of the PL intensity is due to recombination of excitons excited at negative times with respect to the laser pulse peak (taken as $t=0$).

After determining τ_r and τ_a to fit (the unpolarized) $I_{\rm PL}(t)$, $\tau_{\rm cir}$ and $\tau_{\rm cir}^0$ are the only adjustable parameters in Eq. (6) when fitting the circular polarization profiles

$$P_{\rm cir}(t)=[A_m^+(t)-A_m^-(t)]/[A_m^+(t)+A_m^-(t)]\ .$$

We fix $\tau_{\rm cir}^0$, and for each of the different curves of Fig. 3(b) we adjust only $\tau_{\rm cir}$ to best fit the experimental profile. The $P_{\rm cir}$ curve fittings are shown by the solid line in Fig. 3(b). The different curves correspond to different (E_l-E_m) separations which are associated with the spin relaxation of excitons with different in-plane wave vectors $\mathbf{K}_\parallel$. We find $\tau_{\rm cir}$ to decrease with the increase of $|\mathbf{K}_\parallel|$ within the $1S$ band. This is expected due to the enhanced band admixture for large-$\mathbf{K}_\parallel$ states.[20,21] When the exciting energy is further increased to the spectral range of $E_l\sim E_{2S}(K_\parallel=0)$, $\tau_{\rm cir}$ increases due to the smaller spin-relaxation rate corresponding to $\mathbf{K}_\parallel\sim 0$ states of the $2S$ band. For the case of linear polarization, $\tau_{\rm lin}^0$ is fixed and $\tau_{\rm lin}$ is similarly adjusted to fit each of the different

$$P_{\rm lin}(t)=[A_m^x(t)-A_m^y(t)]/[A_m^x(t)+A_m^y(t)]$$

profiles of Fig. 3(c). Here, too, we find $\tau_{\rm lin}$ to decrease with increasing $|\mathbf{K}_\parallel|$ within the $1S$ band and then increase when $E_l\sim E_{2S}(K_\parallel=0)$. The fits to the linear polarizations are shown by the solid lines in Fig. 3(c). The best fitted $\tau_{\rm cir}$ and $\tau_{\rm lin}$ (using a fixed $\tau_{\rm cir}^0=\tau_{\rm lin}^0=600$ ps) are shown in Fig. 1(b) as a function of E_l.

The polarization decay curves ($P_{\rm cir}$ and $P_{\rm lin}$) are extracted from polarized PL measurements like those in Fig. 2. The polarized PL decay curves are characterized by relaxation times (τ_a and τ_r) greater than 120 ps and are thus measured quite accurately by our system. However, difference curves obtained from subtracting two such polarized PL curves can reveal information on much shorter relaxation times. The time resolution of these difference curves is not determined by the system decay time. It is the system noise figure which determines the system's ability to differentiate between two long relaxation times differing by a small amount. We estimate this to be on the order of 5 ps for our measurements. $P_{\rm cir}$ and $P_{\rm lin}$, which are just normalized difference curves, can thus reveal relaxation times as short as 5 ps.

For both circular and linear polarizations, we find that the fit is not very sensitive to $\tau_{\rm cir}^0$ and $\tau_{\rm lin}^0$, respectively. A good fit can be obtained for a wide range of $\tau_{\rm cir}^0$ and $\tau_{\rm lin}^0$ varying from 300 to 1000 ps. Using a fixed $\tau_{\rm cir}^0=\tau_{\rm lin}^0=600$ ps, the theoretical profiles using Eqs. (5) and (6) are fitted to the experimental curves of Figs. 3(b) and 3(c). This determines $\tau_{\rm cir}$ and $\tau_{\rm lin}$ as the only fit parameter very sensitively, since the relaxation times τ_a and τ_r are deter-

mined separately [Fig. 3(a)]. The solid lines of Figs. 3(b) and 3(c) represent the theoretical curve fitting best the experimental profile. Theoretical profiles calculated for different values of τ_{cir} or τ_{lin} clearly deviate from the experimental profiles when τ_{cir} or τ_{lin} is changed by more than $\pm 15\%$. τ_{cir} and τ_{lin} are determined this way for a given set of τ_a, τ_r, and τ^0_{cir} or τ^0_{lin}, respectively. However, each of the τ_a, τ_r, and τ^0_{cir} or τ^0_{lin} relaxation times themselves can vary within some range and still maintain good fits to the PL and polarization decay curves. Determining τ_{cir} and τ_{lin} to best fit the experimental curves for various sets of τ_a, τ_r, and τ^0_{cir} or τ^0_{lin} gives τ_{cir} and τ_{lin} values differing by up to $+100\%$ and -50% relative to those shown in Fig. 1(b). However, for every given set of possible τ_a, τ_r, τ^0_{cir}, and τ^0_{lin}, τ_{cir} and τ_{lin} give a clearly observed trend, showing the 1*S*-2*S* behavior (as a function of E_l) as shown in Fig. 1(b).

The experimentally determined $\tau_a(E_l)$,$\tau_{cir}(E_l)$, and $\tau_{lin}(E_l)$ plotted in Fig. 1(b) allow us to better realize their dependence on the exciton kinetic energy $(E_l - E_m)$. A physical insight into the relative electron and hole relaxation rates can be gained by the following analysis. Assuming that the hole spin relaxation is much faster than that of the electron, the circular polarization relaxation time τ_{cir} is limited by the electron spin relaxation and can be approximated by

$$\frac{1}{\tau_e} \approx \frac{1}{\tau_{cir}} . \tag{7}$$

P_{lin}, on the other hand, is a property of the *e-h* pair, and any depolarizing process that either one of the particles undergoes or loss of the spin coherence between them will destroy the whole pair polarization. τ_{lin} thus reflects the spin relaxation of either the electron or the hole or the loss of the *e-h* spin coherence due to some other spin coherence relaxation process:

$$\frac{1}{\tau_{lin}} \approx \frac{1}{\tau_e} + \frac{1}{\tau_h} + \frac{1}{\tau'_{SC}} . \tag{8}$$

τ_h is the hole spin-relaxation time and τ'_{SC} is the *e-h* spin coherence relaxation time which is due to all other processes apart from the electron and the hole spin relaxation. Assuming now that the fastest spin coherence relaxation process is the hole spin relaxation, i.e., $\tau_h \ll \tau'_{SC}$, and using Eqs. (7) and (8) we find

$$\frac{1}{\tau_h} \approx \frac{1}{\tau_{lin}} - \frac{1}{\tau_{cir}} . \tag{9}$$

In an exciton the electron and the hole parts of the excitonic wave function are superpositions of plane-wave states spanning a range of wave vectors $\sim 1/2a_B$, where a_B is the exciton Bohr radius. Thus the electron and the hole parts of the excitonic wave function can be described by one-particle wave packets centered around k_e and k_h, respectively. Throughout this paper k_e and k_h denote the center values of such one-particle wave packets rather than simply plane waves. Since both the electron and the hole have nearly the same group velocity (which is equal to the exciton group velocity),

$$\frac{\hbar k_e}{m_e} = v_e \approx v_h = \frac{\hbar k_h}{m_h} . \tag{10}$$

For the in-plane electron and hole effective masses we have $m_h \approx 2.2 m_e$; thus we obtain $k_h \approx 2.2 k_e$. Since

$$\left[\frac{2M_{ex}(E_l - E_m)}{\hbar^2} \right]^{1/2} = K_{\parallel} = k_e + k_h , \tag{11}$$

we can calculate $\tau_e(k_e)$ and $\tau_h(k_h)$ from the fitted $\tau_{lin}(K_{\parallel})$ and $\tau_{cir}(K_{\parallel})$ shown in Fig. 1(b). In Fig. 5 we show the resulting $\tau_e(k_e)$ and $\tau_h(k_h)$. The error bars reflect the possible $\pm 15\%$ error in τ_{cir} and τ_{lin} when they are determined for a given set of τ_a, τ_r, τ^0_{cir}, and τ^0_{lin}. Using various other possible sets of values for τ_a, τ_r, τ^0_{cir}, and τ^0_{lin} will give τ_{cir} and τ_{lin} and thus τ_e and τ_h values differing by up to $+100\%$ and -50% relative to those shown in Fig. 5. However, here too, for every given set of possible τ_a, τ_r, τ^0_{cir}, and τ^0_{lin}, τ_e and τ_h give a clearly observed trend. Both τ_e and τ_h decrease with the increase in $k_{\parallel}$ and the ratios between the various $\tau_e(k_e)$ and $\tau_h(k_h)$ values are similar to those shown in Fig. 5. The obtained $\tau_h(k_h)$ is is good agreement with the impurity-assisted spin-flip scattering times calculated by Ferreira and Bastard.[21] They assumed scattering by ionized impurities ($N_{imp} = 10^{10}$ cm^{-2}) localized on one interface of the quantum well. This assumption is in agreement with our model suggesting that the depolarization is due to elastic scattering processes which occur while the exciton moves in the island where it recombines. The very large τ^0_{lin} that we find corresponds to a long spin-relaxation time of $k_h = 0$ holes, and this agrees well with the calculations of Ref. 21. $\tau_e(k_e)$, however, is surprisingly short when compared to $\tau_h(k_h)$ considering the small k_e in-

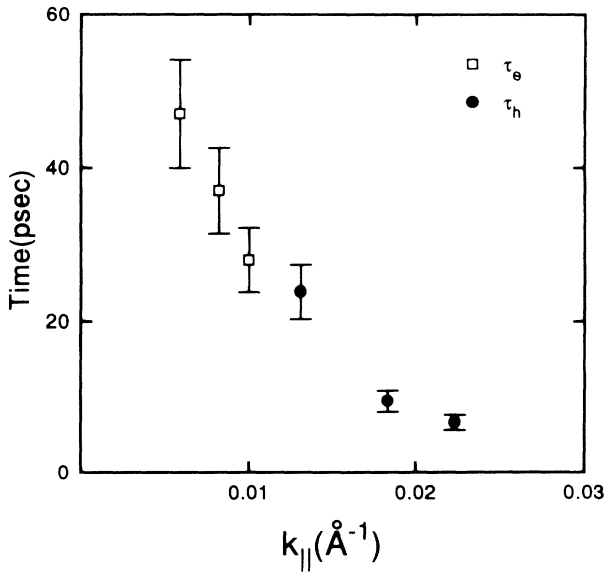

FIG. 5. In-plane wave-vector dependence of the spin-relaxation times of the hole part and electron part of the excitonic wave function.

volved. Figure 5 shows that an electron and hole having similar k values have similar spin-relaxation times, whereas early works[14] have always assumed a much faster hole spin-relaxation time. In addition, it is much smaller than that of free electrons [$\sim 0.15-10$ ns (Refs. 16, 28)]. These fast electron spin-relaxation times can be understood as due to the strong e-h exchange interaction within the exciton[16,28,29] which decreases the electron spin-relaxation time. Recently reported temperature-dependent spin-relaxation times of excitons in high magnetic fields in $GaAs/Al_xGa_{1-x}As$ QW's support this conclusion of e-h exchange interaction as the dominant spin-relaxation mechanism.[30] Note, however, that our earlier assumption of a faster hole spin-relaxation time relative to that of the electron still holds, since for a given excitonic $K_{\parallel}$ state $\tau_e \sim 3\tau_h$. In Fig. 5 the excitonic states corresponding to the larger values of τ_h correspond also to the larger values of τ_e.

IV. SUMMARY

In conclusion, we have compared the time dependence of the degrees of linear and circular polarization $P_{\rm lin}$ and $P_{\rm cir}$ of $(e1{:}{\rm hh}1)1S$ excitons excited at different energies within the excitonic band. We interpret these results by assuming that delocalized excitons can be described by a well-defined in-plane wave vector $K_{\parallel}$. We show that the $K_{\parallel}$ dependence of the excitonic energy-relaxation time τ_a, the exciton spin-relaxation time $\tau_{\rm cir}$, and the exciton alignment-relaxation time $\tau_{\rm lin}$ can account well for the PL and the polarization decay curves. These relaxation times can be assumed to be determined by the spin-relaxation times of the individual electron and hole in the exciton, τ_e and τ_h, respectively. Assuming that k_e and k_h are the wave vectors of the center wave packets that build the exciton with $K_{\parallel}$, we estimate experimentally $\tau_e(k_e)$ and $\tau_h(k_h)$. $\tau_h(k_h)$ is in good agreement with the calculation of Ref. 21 based on impurity-assisted spin-flip scattering. We conclude that the hole part of the excitonic wave function depolarizes primarily by elastic scattering processes which occur while the exciton moves over large-scale interface islands. Electrons within an exciton relax their spin state much faster than free electrons and much faster than expected when compared to the spin relaxation of the hole part of the excitonic wave function. We attribute this to the strong e-h exchange interaction between the electron and hole components of the exciton.

ACKNOWLEDGMENTS

The work at Technion was supported by the United States–Israel Binational Science Foundation (BSF), Jerusalem, Israel and was done at the Barbara and Norman Seiden Center for Advanced Opto-Electronics Research. Two of the authors (A.R. and E.C.) acknowledge the support of the Fund for the Promotion of Research at the Technion.

*Present address: AT&T Bell Laboratories, Murray Hill, NJ 07974.

[1] J. Feldman, G. Peter, E. O. Gobel, P. Dawson, K. Moore, C. Foxon, and R. J. Elliot, Phys. Rev. Lett. **59**, 2337 (1987).
[2] H. Wang, M. Jiang, and D. G. Steel, Phys. Rev. Lett. **65**, 1255 (1990).
[3] H. Hillmer, A. Forchel, S. Hansman, M. Morohashi, E. Lopez, H. P. Meier, and K. Ploog, Phys. Rev. B **39**, 10 901 (1989).
[4] T. C. Damen, J. Shah, D. Y. Oberli, D. S. Chemla, J. E. Cunningham, and J. M. Kuo, Phys. Rev. B **42**, 7434 (1990).
[5] T. Takagahara, Phys. Rev. B **31**, 6552 (1985).
[6] J. Christen and D. Bimberg, Phys. Rev. B **42**, 7213 (1990); J. Christen, Festörperprobleme **30**, 239 (1990).
[7] R. F. Schnabel, R. Zimmermann, D. Bimberg, H. Nickel, R. Losch, and W. Schlapp, Phys. Rev. B **46**, 9873 (1992).
[8] M. Zachau, J. A. Kash, and W. T. Masselink, Phys. Rev. B **44**, 8403 (1991).
[9] J. Hegarty and M. D. Sturge, J. Opt. Soc. Am. B **7**, 1143 (1985).
[10] A. Honold, L. Schultheis, J. Kuhl, and C. W. Tu, Appl. Phys. Lett. **52**, 2105 (1988).
[11] A. Honold, L. Schultheis, J. Kuhl, and C. W. Tu, Phys. Rev. B **40**, 6442 (1989).
[12] *Optical Orientation*, edited by F. Meier and B. P. Zakharchenya (North-Holland, Amsterdam, 1984). The papers by M. I. Dyakonov and V. I. Perel' (p. 11) and by G. E. Pikus and A. N. Titkov (p. 73) are reviews of free-carrier optical spin orientation. The paper by R. Planel and C. Benoit à la Guillaume (p. 353) is a review of optical orientation and alignment of excitons.
[13] G. E. Pikus and E. L. Ivchenko, in *Excitons*, edited by E. I. Rashba and M. D. Sturge (North-Holland, Amsterdam, 1982), p. 205.
[14] R. C. Miller and D. A. Kleinman, J. Lumin. **30**, 520 (1985).
[15] V. A. Chitta, E. C. F. da Silva, D. Toet, M. Potemski, J. C. Maan, and K. Ploog (unpublished).
[16] T. C. Damen, L. Viña, J. E. Cunningham, and J. Shah, Phys. Rev. Lett. **67**, 3432 (1991).
[17] Ph. Roussignol, P. Rolland, R. Ferreira, C. Delalande, G. Bastard, A. Vinattieri, L. Carraresi, M. Coloci, and B. Etienne, Surf. Sci. **267**, 360 (1992).
[18] J. B. Stark, W. H. Knox, and D. S. Chemla, Phys. Rev. Lett. **68**, 3080 (1992).
[19] S. Bar-Ad and I. Bar-Joseph, Phys. Rev. Lett. **68**, 349 (1992).
[20] T. Uenoyama and L. J. Sham, Phys. Rev. Lett. **64**, 3070 (1990).
[21] R. Ferreira and G. Bastard, Phys. Rev. B **43**, 9687 (1991).
[22] A. Bonnot, R. Planel, and C. Benoit à la Guillaume, Phys. Rev. B **9**, 690 (1974).
[23] H. Stolz, D. Schwarze, W. von der Osten, and G. Weimann, Superlatt. Microstruct. **6**, 271 (1989).
[24] A. Frommer, E. Cohen, Arza Ron, and L. N. Pfeiffer, Phys. Rev. B **48**, 2803 (1993).
[25] J. E. Zucker, A. Pinczuk, D. S. Chemla, and A. C. Gossard, Phys. Rev. B **35**, 2892 (1987).
[26] D. Gammon, B. V. Shanabrook, and D. S. Katzer, Phys. Rev. Lett. **67**, 1547 (1991).
[27] B. M. Ashkinadze, E. Cohen, Arza Ron, and L. N. Pfeiffer, Phys. Rev. B **47**, 10 613 (1993).
[28] M. J. Snelling, A. S. Plaut, G. P. Flinn, A. C. Tropper, R. T. Harley, and T. M. Kerr, J. Lumin. **45**, 208 (1990).
[29] M. J. Snelling, E. Blackwood, R. T. Harley, P. Dawson, and C. T. B. Foxon (unpublished).
[30] V. A. Chitta, M. Potemski, J. C. Maan, A. Fasolino, K. Ploog, and G. Weimann, Superlatt. Microstruct. **9**, 303 (1991).